JOURNAL OF AGRICULTURAL AND FOOD CHEMISTRY

Structural Characterization, Physicochemical Properties, Suspension Stability, and Adsorption Properties of Four Solid Forms of Amitraz

MELGARDT M. DE VILLIERS,*,† CHARMAINE M. VAN EEDEN,‡ WILNA LIEBENBERG,‡ MINGNA SONG,† WILLIAM M. KOLLING,† AND MINO R. CAIRA§

Department of Basic Pharmaceutical Sciences, School of Pharmacy, University of Louisiana at Monroe, Monroe, Louisiana 71209, Research Institute for Industrial Pharmacy, School of Pharmacy, North-West University, Potchefstroom 2520, South Africa, and Department of Chemistry, University of Cape Town, Rondebosch 7701, South Africa

This paper reports the identification and preparation of three crystalline (A−C) and one metastable form (D) of amitraz. These were identified by their crystal morphology, crystal structures, aqueous solubility, and thermal properties. Form C was the least soluble (7 μg/mL) and had the highest melting point (115 °C). The differences in melting point (82 vs 72 °C) and solubility (20 vs 23 μg/mL) of forms A and B were not significant. The metastable noncrystalline form D (Tg = 38 °C, transition temperature = 62 °C, and melting point = 78 °C) was obtained by deposition on the surface of activated carbon from acetonitrile solutions. When the anionic surfactant sodium lauryl sulfate was added to the solubility medium, the solubilities of forms A and B were increased 10−11-fold and that of form C was increased 28-fold. Changing the crystal form had an effect on the stability of amitraz suspensions. Form C was the most stable with a $t_{1/2}$ of 136 days, and form B was the least stable with a $t_{1/2}$ of 28 days. The stability correlated with solubility differences. The addition of sodium lauryl sulfate to the suspensions increased the rate of hydrolysis (mean $t_{1/2}$ = 17 h), and because of increased solubility, there was no difference in the stability of the crystal forms in the anionic surfactant solution.

KEYWORDS: Amitraz; polymorphs; stability; solubility

INTRODUCTION

Amitraz, **Figure 1**, is a formamide insecticide developed for use on deciduous fruit and citrus mites, and it is also used as an alternative to coumaphos, an organophosphate, for tick eradication on cattle. Amitraz and its hydrolysis product 2,4-dimethylaniline are known to be toxic (*1*−*3*). Pollution of rivers and streams by amitraz can also occur when freshly treated cattle enter streams to drink or to cross after being dipped or from the runoff from the area surrounding the dip vat (*4*).

The fate of amitraz in the aquatic environment was investigated previously by Allen and Arnold (*5*), who reported that the pesticide dissipated from the water through hydrolysis and adsorption by the sediment. Pierpoint et al. (*6*) and Van Eeden et al. (*7*) studied the kinetics and basic mechanisms of amitraz hydrolysis as well as the effect of cosolvents and metal ions. In these studies, it was found that amitraz was readily hydrolyzed under acidic conditions forming two acid stable compounds. Zaranyika and Mandizha (*8*) studied the adsorption/desorption of amitraz by suspended river sediment particles in an aqueous medium in terms of a model, which assumes an adsorption/desorption equilibrium. Their results illustrated that amitraz does participate in environmentally important adsorption processes.

Amitraz is a poorly water soluble compound, and to a large extent, its stability in the environment and products depends on its solubility. Solubility also depends on the crystal form. The existence of more than one crystal form of the same material, known as polymorphism, or the formation of solvates can result in different physical properties such as density, melting point, hygroscopicity, and solubility (*9*, *10*). These solid forms include crystalline polymorphs (i.e., solids having the same chemical composition but different crystal structures), solvates (cocrystals of the drug and solvent molecules), isomorphic desolvates (produced by loss of solvent while the initial solvate structure is retained), and amorphous solids.

Although very little is published about the crystal properties of pesticides, as far back as 1946, McIntosh et al. (*11*) related crystal size and shape to the contact toxicity of DDT suspensions. In this paper, the results of a study focused on the preparation and characterization of amitraz polymorphs are

* To whom correspondence should be addressed. Tel: 318-342-1727. Fax: 318-342-1737. E-mail: devilliers@ulm.edu.
† University of Louisiana at Monroe.
‡ North-West University.
§ University of Cape Town.

10.1021/jf048915a CCC: $27.50 © 2004 American Chemical Society
Published on Web 11/05/2004

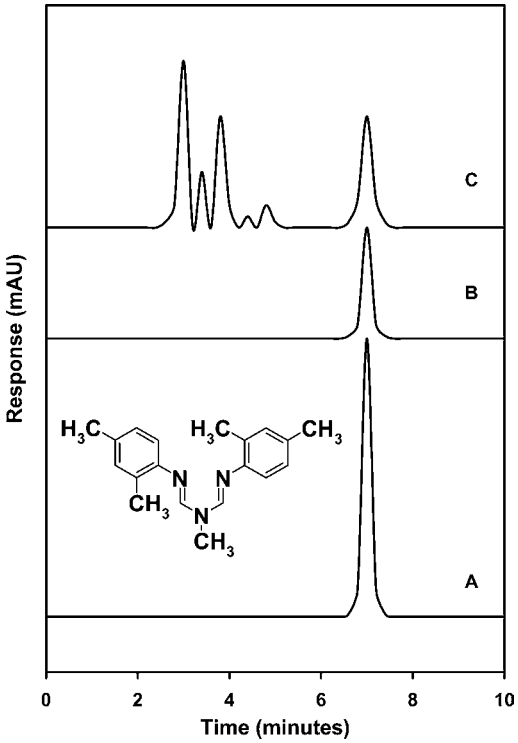

Figure 1. HPLC chromatograms of amitraz: (**A**) 150 μg/mL, (**B**) 50 μg/mL, and (**C**) acidified standard solution left overnight at 40 °C. Insert shows the molecular structure of amitraz (MW = 293.41).

reported. Differences in the solubility and physical, thermodynamic, and chemical stabilities of the polymorphs were also determined.

MATERIAL AND METHODS

Materials. Amitraz standard and an amitraz sample were obtained from Logos Agvet (Midrand, South Africa). The mean assay of the raw material was 99.7% with a mean volume particle size of 44 ± 2.1 μm. Reagent grade chemicals and high-performance liquid chromatography (HPLC) grade acetonitrile were obtained from Spectrum Chemicals (St. Louis, MO) or Saarchem (Krugersdorp, South Africa). HPLC grade water was used throughout the study. The activated carbon (Darco KB-B, Norit, Marshall, TX) had a mean surface area (BET) of 1500 m^2/g, a bulk density of 0.42 g/mL, a surface pH of 4.5−6.5, and a mean volume particle size of 43 μm (d90 < 125 μm).

Thermal Analysis. Thermal analysis methods used in this study included differential scanning calorimetry (DSC) and thermogravimetric analysis (TGA). DSC traces were recorded with a DSC 2920 modulated DSC (mDSC) (TA Instruments, New Castle, DE). The DSC was calibrated for temperature and enthalpy using the melting temperature of highly pure indium standard. Samples weighing 3−5 mg were heated in crimped aluminum cells at a rate of 10−20 K/min under nitrogen gas flows of 35 mL/min. mDSC analysis using the reversing signal was used in an attempt to distinguish the melting points of closely melting mixtures of the polymorphs. About 10 mg samples were accurately weighed and thermally scanned between 0 and 120 °C in aluminum pans with pinholes. The scanning conditions included a heating ramp of 1 °C/min with the modulation amplitude of 1 °C in a 60 s period. TGA analysis was performed on all samples indicated by DSC as being possible solvates or hydrates. TGA traces were recorded with a Hi-Res Modulated TGA 2950 (TA Instruments). The sample weight was approximately 5−8 mg, and heating rates of 1−12 K/min under nitrogen gas flows of 35 mL/min were used.

Preparation of Crystal Forms. Saturated solutions of amitraz in the different solvents were prepared by heating the solutions (not exceeding 60 °C) under constant stirring and nitrogen purge until the majority of the amitraz was dissolved. The solutions were filtered, sealed, and stored at room temperature or refrigerated until crystallization was completed. The crystals were stored in these solutions, and before analysis, the crystals were placed on filter paper and dried under vacuum in a desiccator over calcium sulfate for 4−12 h (W. A. Hammond DRIERITE Co. LTD, Xenia, OH). All crystals were used within 72 h of preparation, and HPLC analysis did not show any significant decomposition following crystallization. A Philips XL 30 scanning electron microscope (Philips, Eindhoven, Netherlands) or Amray (Amray Pty. Ltd., Bedford, MA) was used to obtain photomicrographs of the various crystal forms. Samples were adhered to a small piece of carbon tape mounted before being coated with a thin gold−palladium film (Eiko Engineering ion Coater IB-2, Ibaraki, Japan).

X-ray Powder Diffraction (XRPD). XPRD patterns were obtained at room temperature on either a Philips PM 9901/00 (Philips) or Bruker D8 Advance diffractometer (Bruker, Rheinstetten, Germany). The isothermal measurement conditions were as follows: target, Cu; voltage, 40 kV; current, 30 mA; divergence slit, 2 mm; anti-scatter slit, 0.6 mm; receiving slit, 0.2 mm; monochromator; detector slit, 0.1 mm; scanning speed, 2°/min (step size 0.025°, step time, 1.0 s). Approximately 300 mg samples were weighed into aluminum sample holders, taking care to avoid introducing preferred orientation of the crystallites. The XRPD diffractograms of the samples were compared with regard to peak position and relative intensity, peak shifting, and the presence or lack of peaks in certain angular regions.

Single-Crystal X-ray Structure Analysis. Prismatic pale yellow crystals were obtained by recrystallization from acetone. Preliminary X-ray photography revealed 2/m Laue symmetry indicating that the monoclinic crystal system and the space group were determined unequivocally from systematic absences. Intensity data were collected using the ω-2θ scan mode on an Enraf-Nonius CAD4 four-circle diffractometer employing graphite-monochromated Mo Kα radiation (λ = 0.71069 Å). Data were corrected for Lorentz and polarization factors (*12*). Accurate unit cell parameters were determined by least-squares refinement based on the angular parameters of 24 reflections in the 2θ range 32−34°. Intensity decay (<1%) was determined by monitoring the intensities of three reference reflections every hour.

Infrared Spectroscopy. IR spectra of powdered samples were recorded on a Nexus 470 spectrophotometer (Nicolet Instrument Corporation, Madison) over a range of 4000−400 cm^{-1} with the KBr disk technique. Amitraz samples weighing approximately 2 mg were mixed with 200 mg of KBr (Merck, Darmstadt, Germany) by means of an agate mortar and pestle. Disks were pressed using a Beckman 00-25 press (Beckman, Scotland) at a pressure of 15 × 10^3 kg/cm^2.

HPLC Analysis. For adsorption and stability testing, amitraz was analyzed by HPLC using a modified stability indicating method described by Tseng et al. (*13*). An HPLC instrument (AS 1000 autosampler and P2000 pump, Thermo Separation Products, Waltham, MA) equipped with a multiple wavelength UV detector (UV 3000 detector) set at a wavelength of detection λ_{max} = 313 nm was used. Chromatographic separation was performed using a C18 column (Econosil, 5 μm sized particles, 250 mm × 4.6 mm, Alltech, Deerfield, IL). The mobile phase was acetonitrile:water (80:20, v/v); flow rate, 1.0 mL/min; injection volume, 20 μL. The retention time for amitraz was 6.7 min, and the limit of detection was 1.0 ng/mL. Results were the mean of three analyses. The HPLC method used in this study complied with the specifications for system suitability for chromatographic methods as required by the United States Pharmacopeia (*14*). One hundred milligrams of amitraz was accurately weighed in a 100 mL volumetric flask and dissolved to volume with acetonitrile. This solution was diluted to prepare standard solutions with final concentrations ranging from 10 to 150 μg/mL. **Figure 1** shows examples of the HPLC chromatograms obtained in this study.

Solubility and Intrinsic Dissolution Measurements. An amount of powder, enough to ensure that supersaturation could be obtained, namely, 10 ± 1 mg, was measured into 5 mL ampules. To each ampule, 5 mL of Milli-Q water or phosphate buffer, pH 5.8, containing 0.5% sodium lauryl sulfate was added, flushed with nitrogen, and sealed. The ampules were rotated at 60 rpm (Heidolph RZR-2000 rotator, Germany) in a thermostatically controlled (Julabo EM/4 thermostat, Germany) water bath at 20−50 (±1) °C. Samples were withdrawn and filtered through a 0.45 μm filter after 24 h. The concentrations of the filtered samples were determined by HPLC. Results obtained from

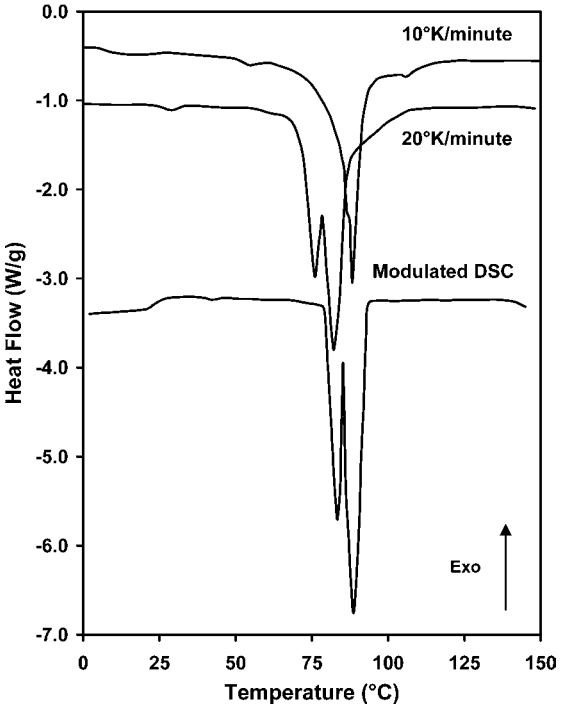

Figure 2. DSC traces of amitraz raw material at different heating rates and using mDSC (the reserving signal).

aqueous solubility studies were compared to identify possible differences between the various polymorphic forms. These results were analyzed statistically using the Newman−Keuls test (Statistica for Windows 5.1B, StatSoft, Inc., Tulsa, OK) to determine the extreme of statistically significant differences. DSC traces of all samples were recorded before and after solubility determination to identify possible polymorphic transformations.

The intrinsic dissolution rate (IDR) was determined by the propeller-driven method as described by Singh et al. (*15*). Powdered samples of the crystal forms were slowly compressed into 12 mm tablets in a die, so that the tablet surface was flush with the die surface (Beckmann Type 00-25 IR press), with a dwell time of 1 min to ensure compaction. A compression force of 2.3×10^5 kg/cm^2 could be used without an appreciable change in the apparent surface area of the disk. The back of the die was sealed, and then, it was placed into a dissolution flask [apparatus 2 of the USP (*14*) with a paddle speed of 100 rpm, VanKel, Cary, NC] containing 500 mL of an ethanol:water (40:60 v/v) mixture as the dissolution medium, kept at 37 ± 1 °C. The amount of drug dissolved as a function of time was determined by HPLC. After compression and at the end of the dissolution, the top layer of some tablets was removed and analyzed by DSC to determine if the crystal form changed during dissolution testing.

Degradation Kinetics of Sorbed and Suspended Amitraz. For degradation studies, amitraz suspensions of the crystal forms, particle size fraction between 25 and 100 μm obtained by sieve screening and a suspension of activated carbon covered with amitraz, were used. Suspensions were prepared in an aqueous buffer solution [0.2 M phosphate buffer, pH 5.8, USP (*14*)] with and without sodium lauryl sulfate added, sealed in ampules, rotated at 60 rpm in a water bath kept at 30 ± 0.5 °C, and analyzed periodically to determine the amount of amitraz remaining. The addition of the sodium lauryl sulfate did not change the pH of the buffer solution. At least three determinations were done for each time point. DSC analysis was used to follow crystal changes during the chemical stability analysis.

RESULTS AND DISCUSSION

The initial melting point determination showed that there were differences in the DSC traces of the amitraz raw material and a reference standard. The standard had one melting endotherm with an onset of melting at around 81−82 °C while the onset

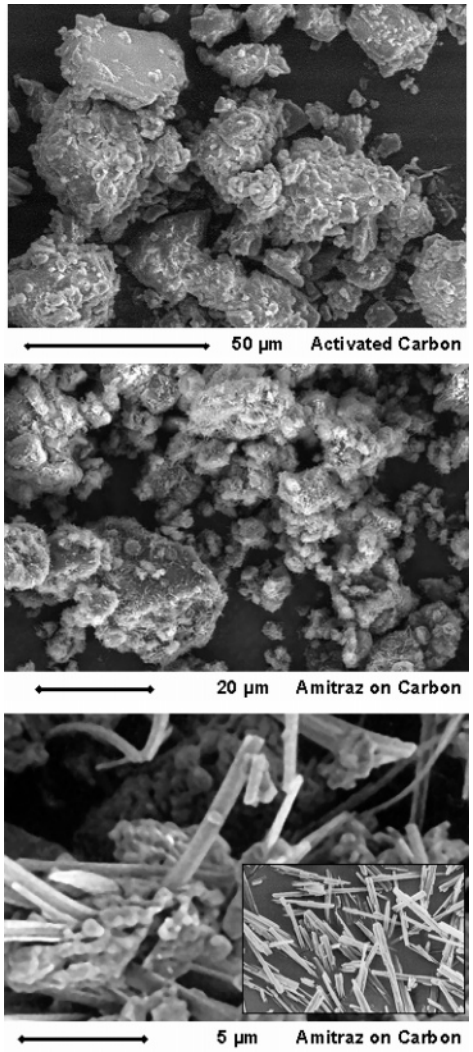

Figure 3. SEM photomicrographs of activated carbon (top), activated carbon covered with amitraz (middle), and close-up of noncrystalline needles growing on the surface of the carbon particles (bottom). Insert on bottom picture is a picture of the needles.

of melting of the raw material was closer to 71−74 °C. Also, the melting endotherm for different samples from the same batch of raw material was not consistent because some melting endotherms had shoulders and appeared to be split peaks (**Figure 2**). Adjusting the DSC heating rate seemed to partially resolve the melting endotherm and clearly showed two overlapping thermal events. Although it was not possible to completely resolve these peaks, mDSC, **Figure 2** (the reversing signal), did separate the peaks enough to indicate two melting points at around 73 and 85 °C (end points).

In addition, adsorption of amitraz to coarse carbon particles led to the deposition of amitraz on the surface of the carbon particles (**Figure 3**). mDSC analysis, **Figure 4** and **Table 1**, showed that the melting point of these amitraz particles was also different from form A. There appeared to be a glass transition temperature around 38−40 °C, followed by the melting of a metastable crystal form at 60−63 °C. Melting of this form leads to the crystallization of crystals that melt at around 78−79 °C, possibly the lower melting crystal form identified in the raw material. This noncrystalline amitraz adsorbed to the carbon particles was not stable because after it was removed from the solvent, dried, and stored at 25 °C, DSC analysis shown in **Figure 4** indicated that a significant amount

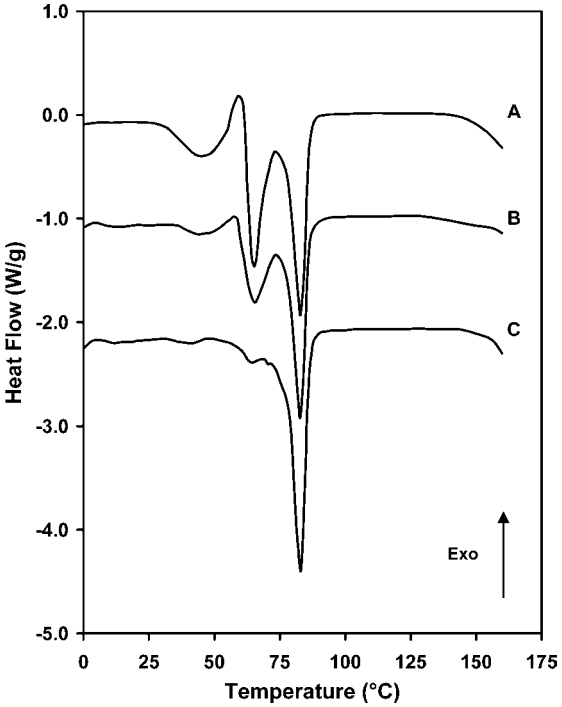

Figure 4. mDSC traces (reversing signal) of amorphous amitraz deposited on activated carbon. (**A**) Immediately after removal from the acetonitrile solution. (**B**) After storage for 7 days at 25 °C in a sealed container. (**C**) After storage for 1 month at 25 °C in a sealed container.

Table 1. Thermal Behavior of the Metastable Amitraz (Form D) Adsorbed on the Activated Carbon ($n = 3$)

	transition		melting point	heat of melting	
Tg (°)	(°C)	(J/g)	(°C)	(J/g)	(J/mol)
38.2 ± 1.85	60.5 ± 0.8	33.9 ± 1.3	78.4 ± 0.9	62.9 ± 3.5	18256 ± 735.4

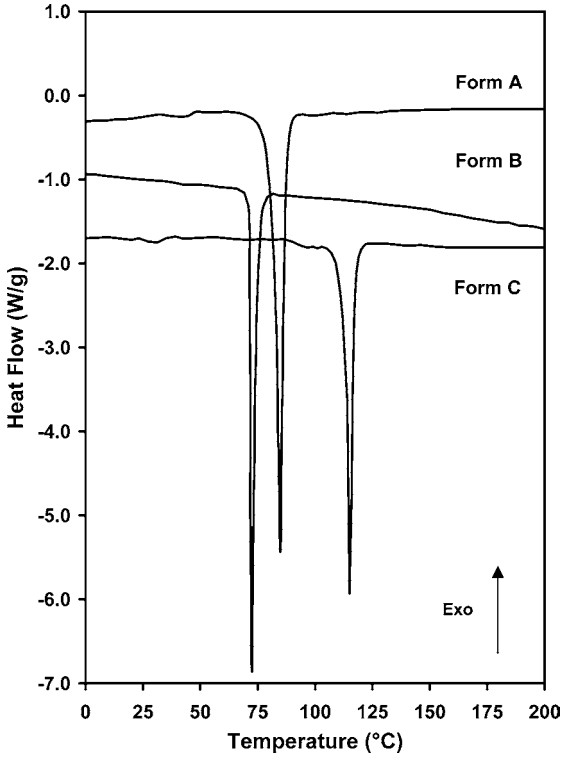

Figure 5. mDSC (reversing signal) traces of the three polymorphs of amitraz.

Table 2. Melting Points (Onset Temperatures) and Enthalpies of Melting for the Three Polymorphs of Amitraz ($n = 3$)

		heat of melting	
crystal form	endotherms (°C)	(J/g)	(J/mol)
form A	82.1 ± 1.2	91.2 ± 4.9	26767 ± 1440.9
form B	71.2 ± 4.4	67.4 ± 6.4	19471 ± 1517.8
form C	115.4 ± 0.7	181.4 ± 7.2	53135 ± 1989.3

was transformed to the higher melting form B after 7 days and almost all after 1 month.

Preparation of Crystal Forms. This unusual thermal behavior of the amitraz prompted a recrystallization study to identify as many amitraz crystal forms as possible. Amitraz is insoluble in water and variably soluble in commonly used organic solvents. Amitraz is also relatively unstable in solution. To improve solution stability, solutions were prepared while nitrogen was bubbled through them. Heated solutions, never exceeding 60 °C, were immediately sealed in 10 mL ampules and allowed to stand until crystallization was complete. This process led to the identification of three crystal forms with distinct melting points (**Figure 5**). All crystals were used within 72 h of preparation, and HPLC analysis did not show any significant decomposition following crystallization. The absence of weight loss for all of the crystal forms observed by TGA analysis indicated that solvates were not formed. The amitraz standard and crystals crystallized from methanol, ethanol, and isopropyl alcohol were named form A. The melting point of this crystal form, **Table 2**, was similar to that reported for amitraz in the literature (*16*).

From acetone and chloroform, a lower melting crystal form, form B, crystallized. The melting point of this form corresponded to the lower melting form identified in the raw material sample. From octanol, *n*-butanol, and propylene glycol, a third crystal form, form C, with a surprisingly high melting point, 115 °C, was crystallized. It was difficult to prepare the last two forms because heat was necessary to prepare sufficiently concentrated solutions, but when these solutions were cooled too fast, form A was produced. Controlled cooling in a thermostatic water bath overcame this problem. Infrared analysis indicated that crystallization did not affect the chemical properties of amitraz. It was not possible to assign differences in the IR spectra to any changes in the crystal forms. The form deposited on the activated carbon could not be reproduced by recrystallization techniques. This form was named form D.

Morphology of the Crystal Forms. Scanning electron microscopic evaluation of the various solid forms (**Figures 3** and **6**) showed significant morphological differences between them. The raw material sample was a mixture of needles, plates, and tabular particles. Form A (the amitraz standard) was primarily composed of prismatic needles. Form B consisted of tabular, isometric crystals. The crystals of form C were also large prismatic needles. The crystal surface of the particles of form C was not very smooth with surface defects that could be the result of irregular crystal growth. The particles of form D were very small (1−2 μm) precipitating on the surface of the activated carbon (**Figure 3**). These particles changed to larger needles upon storage that could be removed from the activated carbon (insert in bottom photomicrograph of **Figure 3**).

Solubility and Dissolution Properties of the Crystal Forms. Solubility analysis of the three crystal forms (**Table 3**) indicated that form B was approximately 1.2 times more soluble than form A and 3.4 times more soluble than form C. This indicated that form B was the most soluble, followed closely by form A

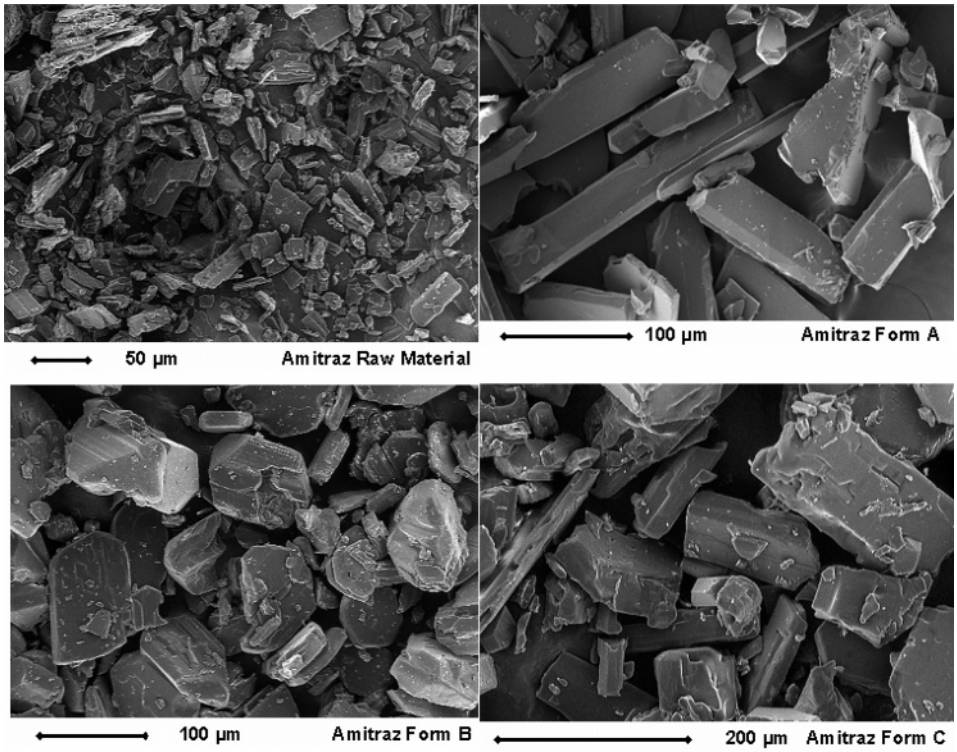

Figure 6. SEM photomicrographs of the amitraz raw material and three crystal forms.

Table 3. Equilibrium Aqueous Solubilities of Amitraz Crystal Forms at Various Temperatures ($n = 3$)

	equilibrium aqueous solubility (μg/mL)		
temperature (°C)	form A	form B	form C
30	19.9 ± 2.0	23.2 ± 1.1	6.9 ± 1.0
35	22.6 ± 1.0	27.9 ± 1.3	8.9 ± 1.0
40	26.8 ± 1.3	31.1 ± 1.6	10.1 ± 0.9
45	31.1 ± 1.5	36.9 ± 1.8	13.5 ± 1.1
50	36.1 ± 1.4	41.3 ± 1.9	16.9 ± 0.6

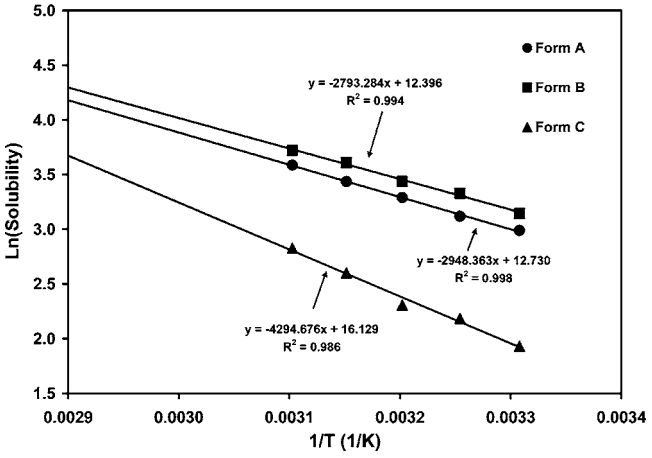

Figure 7. Solubility of different amitraz crystal forms in water, as a function of temperature.

while form C was significantly less water soluble. Aqueous solubilities as a function of increasing temperatures are listed in **Table 3**. The metastable to stable solubility ratios stayed relatively constant over the range of temperatures tested. According to the van't Hoff plots, **Figure 7**, good linearity was observed between the temperature and the solubility data for each crystal form. Within the limited temperature range that the solubility was tested, it was not possible to estimate the transition temperatures where the crystal forms have equal solubilities. However, the data showed that hypothetical transition temperatures would be much higher than the melting point of the most stable form C, 115 °C. The thermodynamic activity of the crystal forms, observed as solubility as a function of temperature, indicated that the amitraz crystal forms are monotropically related (*17*).

A general form of the van't Hoff equation is $\ln C_s = -\Delta H^{\theta}/RT + c$ and plots of $\ln C_s$ against $1/T$ are linear, **Figure 7**, with a slope of $-\Delta H^{\theta}/R$ from which the heats of solution can be estimated. The heats of solution calculated from the slopes of the lines in **Figure 7** were 24.6, 23.2, and 35.8 kJ/mol for forms A, B, and C, respectively. These values are of the same order of magnitude as the heat of melting, ΔH^{f}, listed in **Table 2** for forms A and B but much lower than the ΔH^{f} of form C. The order of thermodynamic stability was the same as estimated from DSC analysis: form C > form A > form B.

By maintaining the dissolution fluid viscosity, the rotational speed of the paddle, and the surface area exposed to the dissolution medium under sink conditions ($C_s \ggg C$), the dissolution rate, $dc/dt = A/V\,K_1C_s$, becomes IDR $= K_1C_s$ where IDR is the IDR, A is the surface area, V is the volume of dissolution medium, K_1 is the rate constant, and C_s is the solubility of the compound. The IDR can be calculated from linear plots of the amount dissolved from a constant surface area vs time and the slopes of the lines divided by the exposed surface area gives the IDR. The IDR's of the three amitraz crystal formed in an ethanol:water (40:60) mixture kept at 37 ± 1 °C were 30.8 μg cm^2/min for form A, 34.7 μg cm^2/min for form B, and 9.8 μg cm^2/min for form C. The dissolution rate of the more soluble form B was approximately 1.1 times that of form A and 3.5 times that of form C. These results reflected to some extent the same trend as the metastable to stable solubility ratios because the order in which the dissolution rate decreased was form C > form A ≥ dorm B.

As a prelude to chemical stability studies, the solubilities of the three crystal forms in buffer, pH 5.8, containing 0.5% sodium

Table 4. Solubilities of the Amitraz Crystal Forms in Phosphate Buffer, pH 5.8, at 30 °C Containing 0.5% Sodium Lauryl Sulfate ($n = 3$)

	form A	form B	form C	form D
solubility (μg/mL)	223.9 ± 10.4	237.3 ± 11.4	198.8 ± 7.2	236.0 ± 5.2

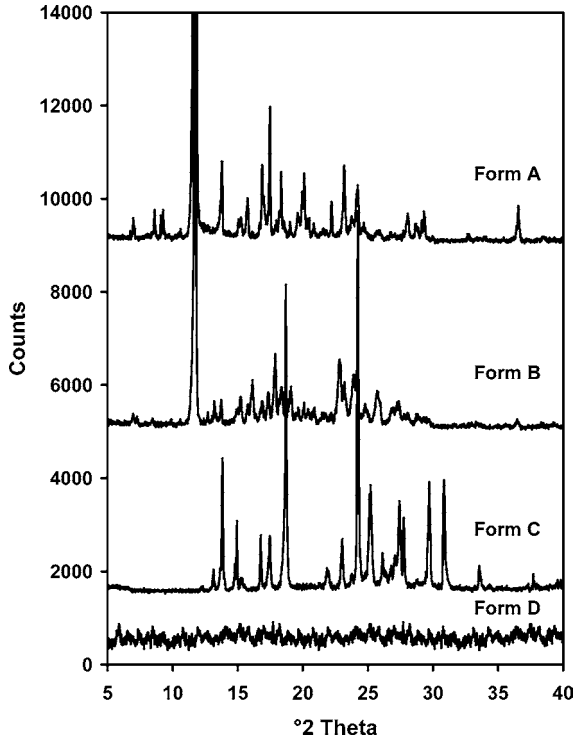

Figure 8. XRPD patterns of the amitraz crystalline forms A, B, A, and the metastable form D.

lauryl sulfate were also measured. The results are listed in **Table 4**. The addition of the surfactant increased the solubilities of forms A and B only between 10 and 11 times but almost 28 times for form C. Although the solubilities were still significantly different ($p < 0.05$), the differences in solubility between the crystal forms compared to the differences in solubility in water were less. The solubility of form D (amitraz deposited on carbon) approached that of form B. This result confirmed the DSC observation made about the thermodynamic stability of this metastable form (**Figure 4**).

Crystal Structures of the Various Forms. The XRPD patterns of the four crystal forms are shown in **Figure 8**. Although the patterns of forms A and B are similar, there are very characteristic peaks that could be used to distinguish them. Form A is characterized by the peaks at 8.62, 9.28, 13.82, 20.10, 23.18, 29.32 °2θ, and form B is characterized by the peaks at 13.20, 15.28, 16.14, 19.10, 22.86, and 25.80 °2θ. Careful inspection of the XRPD pattern of the raw material (**Figure 9**) showed that it was a mixture of forms A and B because the characteristic peaks for the two forms were easily identifiable. XRPD analysis of the amitraz on the carbon surface (**Figure 8**) did not detect any sharp diffraction peaks. This confirmed that the material growing on the surface of the activated carbon was not crystalline.

According to the Merck Index (*16*), amitraz (form A) consists of white monoclinic needles with a melting point between 86 and 87 °C. The actual report of this structure could not be found in the literature. In our study, the quality of crystallized forms A and C was never sufficient enough to do single-crystal structure analysis. However, the single-crystal structure of form

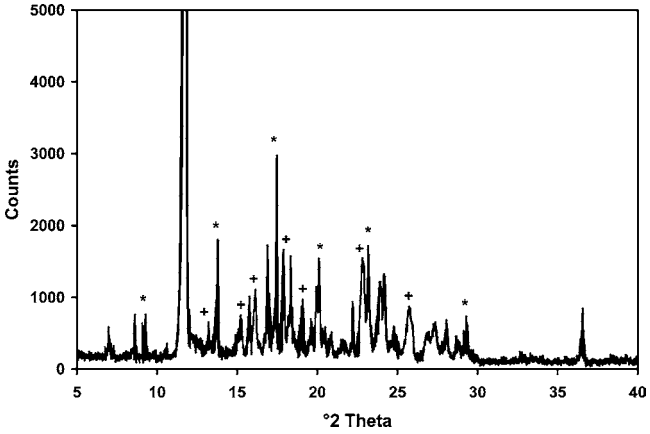

Figure 9. XRPD pattern of amitraz raw material. Peaks marked by * are characteristic for form A and peaks marked by + are characteristic for form B.

Table 5. Crystal Data and Refinement Parameters

chemical formula	$C_{19}H_{23}N_3$
formula weight	293.41
D_{calcd} (g cm^{-3})	1.131
crystal system	monoclinic
space group	$P2_1/c$
a (Å)	11.994(2)
b (Å)	7.631(1)
c (Å)	37.681(9)
β (°)	91.70(2)
V (Å^3)	3447(1)
F(000)	1264
formula units, Z	8
μ (Mo Kα) (mm^{-1})	0.068
crystal size (mm^3)	0.28 × 0.28 × 0.31
T (K)	294(2)
θ min, max	1.12, 25.0
reflections measured	6137
unique reflections	6034
R_{int}	0.019
observed data $I > 2\sigma(I)$	2755
parameters varied	408
R (on F)	0.054
wR (on F^2)	0.161
goodness of fit, S	0.866
Δ/σ mean, max	0.002, 0.105
$\Delta\rho$ min, max (e Å^{-3})	–0.16, 0.17

B was also solved. The structure was solved by direct methods, which revealed two independent molecules in the asymmetric unit (*18*). Refinement was performed against F^2 using full-matrix least-squares methods (*19*). All H atoms were located in difference electron density maps. They were included in idealized positions with isotropic temperature factors equal to 1.2 times those of their parent atoms. All nonhydrogen atoms were refined anisotropically. In the final cycles of refinement, a weighting scheme of the form $w = 1/[\sigma^2(F_o)^2 + (aP)^2 + bP]$, $P = [\max(F_o^2, 0) + 2F_c^2]/3$ was employed. Crystal data and refinement details are listed in **Table 5**.

Figure 10a shows the two independent molecules of amitraz in the asymmetric unit of form B with their atomic numbering and thermal ellipsoids drawn at the 50% probability level (*20*). In both molecules, the triazapentadiene units are essentially planar (**Table 6**) while the xylyl moieties are tilted symmetrically to minimize steric repulsion between hydrogen atoms, as is evident from the space-filling diagram (**Figure 10b**). The formal double bonds (N9−C10 and equivalents) are in the range 1.265(3)−1.273(3) Å while the formal single bonds (C10−N11 and equivalents) are in the range 1.364(3)−1.370(3) Å.

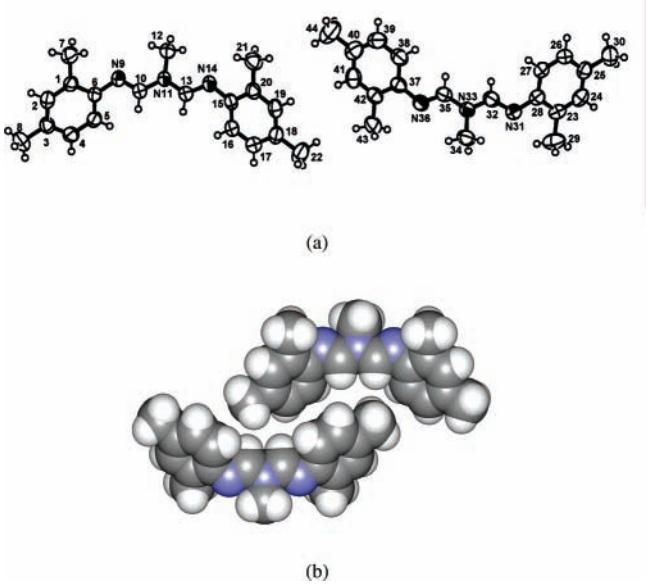

Figure 10. (**a**) Two independent amitraz molecules in the asymmetric unit of form B. (**b**) Space-filling diagram showing molecular conformations.

Table 6. Selected Torsion Angles (deg) Describing the Molecular Conformations

C6–N9–C10–N11	177.4(2)	C28–N31–C32–N33	–174.7(2)
N9–C10–N11–C13	176.8(2)	N31–C32–N33–C35	179.3(2)
C10–N11–C13–N14	–178.6(2)	C32–N33–C35–N36	178.4(2)
N11–C13–N14–C15	–173.5(2)	N33–C35–N36–C37	–179.5(2)
C5–C6–N9–C10	–46.7(3)	C27–C28–N31–C32	38.2(4)
C16–C15–N14–C13	35.9(4)	C38–C37–N36–C35	–45.1(3)

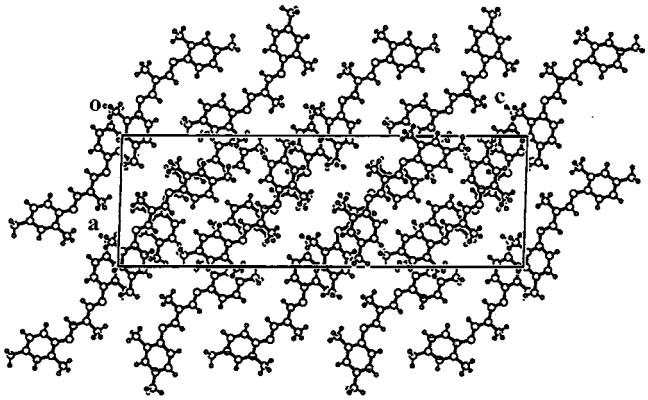

Figure 11. Crystal packing of form B viewed down [010].

Crystal packing for form B is shown in **Figure 11**. Cohesion is maintained by van der Waals interactions and one strong $\pi-\pi$ interaction (3.083 Å) involving the phenyl ring C(1)→C(6) and its symmetry equivalent at $2 - x$, $2 - y$, $-z$. The molecules are arranged in ribbons associated with the (104) crystal planes. The peak at $2\theta = 11-12°$ in the X-ray powder pattern computed from the single crystal data and in the experimental pattern (**Figure 9**) corresponding to reflection from these planes consequently had the highest intensity. The refined unit cell data, atomic positions, thermal parameters, and space group data for the crystal were used as input to the program LAZY PULVERIX (*21*) to generate the idealized XRPD pattern for Cu Kα radiation ($\lambda = 1.5418$ Å). The experimental pattern (**Figure 9**) was in good agreement with the computed pattern.

Stability in Suspension of the Crystal Forms. It is important to know the stability of amitraz in solution but also in the solid state. For this reason, the stability of suspensions prepared with

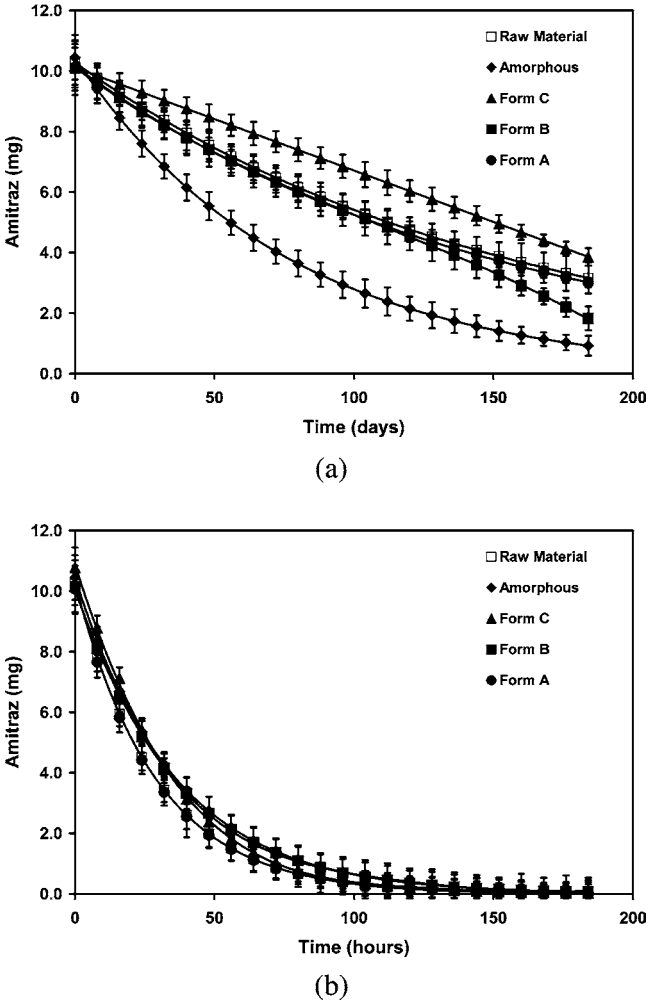

Figure 12. Amount vs time hydrolysis plots for amitraz suspensions in (**a**) aqueous phosphate buffer, pH 5.8, and (**b**) phosphate buffer, pH 5.8, containing 0.5% sodium lauryl sulfate.

Table 7. Effect of Crystal Form on the Degradation of Amitraz Suspended in Aqueous Vehicles with and without Anionic Surfactants

	buffer pH 5.8		0.5% SLS	
crystal form	k_{obs} (days^{-1})	$t_{1/2}$ (days)	k_{obs} (h^{-1})	$t_{1/2}$ (h)
raw material	6.41×10^{-3}	108	3.89×10^{-2}	18
form A	6.60×10^{-3}	105	3.81×10^{-2}	18
form B	8.33×10^{-3}	83	4.42×10^{-2}	16
form C	5.10×10^{-3}	136	4.40×10^{-2}	16
form D	13.18×10^{-3}	53	4.30×10^{-2}	16

the crystal forms (sieve fraction 50−150 μm, 10 mg/5 mL) in phosphate buffer, pH 5.8, with and without 0.5% sodium lauryl sulfate was determined at 30 °C. In **Figure 12a**, the hydrolysis of amitraz as a function of time is shown and hydrolysis rate constants and half-lives are listed in **Table 7**. The results show that there was a correlation between the solubility and the degradation of the amitraz crystal forms. The more soluble forms B and D degraded significantly faster than the poorly soluble form C. DSC analysis showed that form D gradually changed to form B and that the decomposition rate decreased more rapidly with time as compared to the other forms (**Figure 12a**). The addition of the solubilizing and degradation enhancer sodium lauryl sulfate significantly increased the rate of hydrolysis of the amitraz crystal forms, **Figure 12b**, and there were no significant differences between the rate constants and the half-lives for the different crystal forms. The addition of

the anionic surfactant significantly increased the solubility of the crystal forms (**Table 7**), and because amitraz is hydrolyzed much faster in solution, it could explain why there was not a significant difference in degradation of the crystal forms in the surfactant solutions.

In conclusion, thermodynamic analysis showed that the thermodynamic stabilities of the four polymorphs prepared and identified in this study were in the order form C > form A ≥ form B > form D. Form A is the commercially available standard that crystallizes as monoclinic crystals. Forms B and C and the existence of amorphous amitraz have not been reported previously. Form D is a metastable form precipitated from solution on the surface of activated carbon from an acetonitrile solution. The single-crystal structure of form B is also reported. This form crystallized as monoclinic crystals (space group $P2_1/c$) crystals, and the computed X-ray powder pattern was used for identifying this form. The chemical stability of the crystal forms in suspension depended on the solubility, and the more soluble forms B and D degraded faster than the less soluble form A. Form C was the least soluble and the most stable. The addition of an anionic surfactant to the suspension medium significantly increased the solubility and degradation of the amitraz crystal forms and completely canceled the effect that differences in the solubility of the crystal forms had on the rate of hydrolysis.

LITERATURE CITED

(1) Jones, R. D. Xylene/amitraz: A pharmacologic review and profile. *Vet. Hum. Toxicol.* **1990**, *32*, 446−448.

(2) Aziz, S. A.; Knowles, C. O. Inhibition of monoamine oxidase by the pesticide chlordimeform and related compounds. *Nature* **1973**, *242*, 417−418.

(3) Benezet, H. J.; Knowles, C. O. Inhibition of rat brain monoamine oxidase by formamidines and related compounds. *Neuropharmacology* **1976**, *15*, 369−373.

(4) Ahrens, E. H.; Davey, R. B.; George, J. E.; Cooksey, L. M. Efficacy and stability of wettable powder amitraz in field and laboratory studies against Boophilus annulatus (Acari: Ixodidae) in south Texas. *J. Econ. Entomol.* **1989**, *82*, 850−853.

(5) Allen, R.; Arnold, D. J. The comparative fate of [^{14}C]-amitraz in different sediment/water types. *Brighton Crop Prot. Conf.—Pests Dis.* **1990**, *3*, 1023−1028.

(6) Pierpoint, A. C.; Hapeman, C. J.; Torrents, A. Kinetics and mechanism of Amitraz hydrolysis. *J. Agric. Food Chem.* **1997**, *45*, 1937−1939.

(7) Van Eeden, C. M.; Liebenberg, W.; du Preez, J. L.; De Villiers, M. M. Solvent and surfactant enhanced solubilization, stabilization, and degradation of amitraz. *J. Environ. Sci. Health B* **2004**, *B39*, 33−51.

(8) Zaranyika, M. F.; Mandizha, N. T. Adsorption of amitraz by a river sediment: Apparent thermodynamic properties. *J. Environ. Sci. Health B* **1998**, *B33*, 235−251.

(9) Byrn, S. R.; Pfeiffer, R. R.; Stephenson, G.; Grant, D. J. W.; Gleason, W. B. Solid-state pharmaceutical chemistry. *Chem. Mater.* **1994**, *6*, 1148−1158.

(10) Yu, L.; Reutzel, S. M.; Stephenson, G. A. Physical characterization of polymorphic drugs: An integrated characterization strategy. *PSTT* **1998**, *1*, 118−127.

(11) McIntosh, A. H. Relation of crystal size and shape to contact toxicity of DDT suspensions. *Nature* **1946**, *158*, 417.

(12) Frenz, B. A. *Structure Determination Package*; Associates Inc.: College Station, Texas, 1982.

(13) Tseng, S.-H.; Chang, P.-C.; Chou, S.-S. Determination of amitraz residues in fruits by high performance liquid chromatography. *J. Food Drug Anal.* **1999**, *7*, 225−232.

(14) *The United States Pharmacopeia 24 and National Formulary 19 (USP)*. United States Pharmacopeial Convention: Rockville, MD, 2000.

(15) Singh, P.; Desai, S. J.; Flanagan, D. R.; Simonelli, A. P.; Higuchi, W. I. Mechanistic study of the influence of micelle solubilization and hydrodynamic factors on the dissolution rate of solid drugs. *J. Pharm. Sci.* **1968**, *57*, 959−965.

(16) *Merck Index*, 13th ed.; Merck: New Jersey, 2001; p 85.

(17) Byrn, S. R.; Pfeiffer, R. R.; Stowell, J. G. *Solid State Chemistry of Drugs*, 2nd ed.; SSCI-Inc., West-Lafayette, IN, 1999; p 20.

(18) Sheldrick, G. M. SHELXS86. In *Crystallographic Computing 3*; Kruger, G. M., Goddard, R., Eds.; Oxford University Press: Oxford, United Kingdom, 1985; pp 175−178.

(19) Sheldrick, G. M. *SHELXL97, Program for the Refinement of Crystal Structures*; University of Göttingen: Germany, 1997.

(20) Zsolnai, L.; Pritzkow, H. *ZORTEP: ORTEP Program for Personal Computer*; University of Heidelberg: Germany, 1994.

(21) Yvon, K.; Jeitschko, W.; Parthe, E. LAZY PULVERIX, A Computer Program for Calculating X-ray and Neutron Diffraction Powder Patterns. *J. Appl. Crystallogr.* **1977**, *10*, 73−74.

Received for review July 1, 2004. Revised manuscript received September 23, 2004. Accepted September 24, 2004. This work was supported by grants from the National Research Foundation (Pretoria, South Africa) and the Louisiana Board of Regents Enhancement Program [LEQSF(2001-02)-ENH-TR-82]. Research support from the University of Cape Town is also acknowledged.

JF048915A